UCRL-JC-129298
PREPRINT

Oxidation of Automotive Primary Reference Fuels in a High Pressure Flow Reactor

H.J. Curran, W.J. Pitz and C.K. Westbrook
Lawrence Livermore National Laboratory
Livermore, CA

C.V. Callahan and F.L. Dryer
Princeton University, Aerospace Engineering
Princeton, NJ

This paper was prepared for submittal to the
Western States Section/Combustion Institute Spring Meeting
University of California, Berkeley
Berkeley, CA
March 23-24, 1998

January 1998

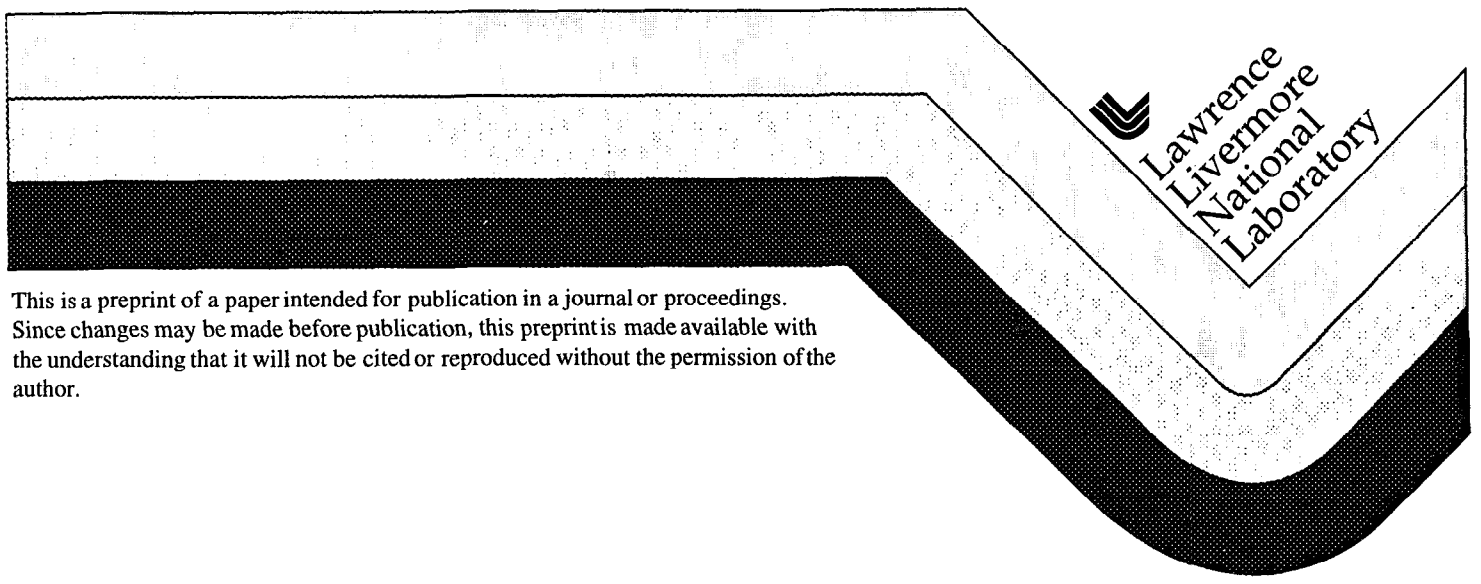

Oxidation of Automotive Primary Reference Fuels in a High Pressure Flow Reactor

H. J. Curran, W. J. Pitz and C. K. Westbrook
Lawrence Livermore National Laboratory, Livermore, CA 94551, USA.

C. V. Callahan and F. L. Dryer
Department of Mechanical and Aerospace Engineering, Princeton University, Princeton, NJ 08544, USA.

Abstract

Automotive engine knock limits the maximum operating compression ratio and ultimate thermodynamic efficiency of spark-ignition (SI) engines. In compression-ignition (CI) or diesel cycle engines the premixed burn phase, which occurs shortly after injection, determines the time it takes for autoignition to occur. In order to improve engine efficiency and to recommend more efficient, cleaner-burning alternative fuels, we must understand the chemical kinetic processes which lead to autoignition in both SI and CI engines. These engines burn large molecular-weight blended fuels, a class to which the primary reference fuels (PRF), n-heptane and iso-octane belong. In this study, experiments were performed under engine-like conditions in a high pressure flow reactor using both the pure PRF fuels and their mixtures in the temperature range 550–880 K and at 12.5 atm pressure. These experiments not only provide information on the reactivity of each fuel but also identify the major intermediate products formed during the oxidation process. A detailed chemical kinetic mechanism is used to simulate these experiments and comparisons of experimentally measured and model predicted profiles for O_2, CO, CO_2, H_2O and temperature rise are presented. Intermediates identified in the flow reactor are compared with those present in the computations, and the kinetic pathways leading to their formation are discussed. In addition, autoignition delay times measured in a shock tube over the temperature range 690–1220 K and at 40 atm pressure were simulated. Good agreement between experiment and simulation was obtained for both the pure fuels and their mixtures. Finally, quantitative values of major intermediates measured in the exhaust gas of a cooperative fuels research engine operating under motored engine conditions are presented together with those predicted by the detailed model.

Introduction

Detailed kinetic mechanisms are needed to understand fully the fundamental chemical processes involved in fuel oxidation and to make intelligent recommendations for additives and replacement compounds which can be used as fuels for automotive engines. This need is emphasized by current limitations in engine operating efficiency, reduced greenhouse gas emissions, and legislative regulation of tailpipe emissions. Kinetic mechanisms must predict properly the key processes that are controlled by chemical reactions in spark-ignition (SI) and compression-ignition (CI) or diesel cycle engine combustion. In SI engines, the chemical kinetic mechanism must predict accurately automotive engine knock which limits the maximum operating compression ratio and ultimate thermodynamic efficiency of the engine. Detailed mechanisms must also predict the partial oxidation of hydrocarbons as they emerge from crevices, a process which leads to raw hydrocarbon emission speciation from SI engines [1, 2]. In CI engines, the kinetic mechanism must accurately predict the premixed burn phase that occurs shortly after injection and determines the time at which autoignition occurs [3].

In this study, a detailed chemical kinetic mechanism has been assembled for the primary reference fuels (PRF) n-heptane and iso-octane. These fuels are used to define the octane reference scale for fully-blended gasolines. The chemistry of n-heptane and iso-octane includes many of the features of large molecular-weight blended fuels. N-heptane is a reactive straight-chain paraffin while iso-octane is a less reactive branched-chain paraffin. Each fuel exhibits richly complex chemistry: at high temperatures fuel decomposition reactions tend to dominate the combustion process while at low temperatures the chemistry is dominated by addition of alkyl radicals to O_2 and subsequent isomerization reactions. Both low and

high temperature chemistry reactions are important for blended fuels used in SI engines and for longer chain (C_{10}–C_{16}) hydrocarbons used in CI engines. However, low temperature chemistry is of even greater importance for fuels burned in CI engines as the higher operating pressures result in a shifting of low temperature chemistry kinetics to higher temperatures. Ultimately our goal is to generate a chemical kinetic mechanism to describe a "surrogate" diesel fuel. Our current "surrogate" fuel lacks representation of the aromatic species, which are an appreciable fraction of conventional diesel fuel. These components will be considered in future work.

Experimental studies of primary reference fuels have been performed in closed vessels [4], flow reactors [5, 6], jet-stirred reactors [7]-[11], shock tubes [12, 13], rapid compression machines [1], [14]-[19] and motored engines [20]-[22]. Ranzi et al. [23, 24] and Côme et al. [25, 26] have generated reduced chemical kinetic mechamisms to describe PRF oxidation at low, intermediate and high temperatures. Roberts et al. [27] used a semi-detailed chemical mechanism which was supplemented by adding a knock subroutine to a quasidimensional spark ignition engine model to simulate iso-octane ignition in a Cooporative Fuels Research (CFR) engine. Detailed mechanisms have also been generated automatically using rules for different reaction classes [28]-[30].

The PRF mechanism developed here must simulate the autoignition phenomena and intermediate product formation at the high pressure conditions found in internal combustion engines. To attain a predictive and validated model, computed results are compared to experimental results at elevated pressures. Predictions of the detailed model are compared to ignition delay times measured in a shock tube [13]. Modeling results are also compared to detailed experimental measurements taken in a high pressure flow reactor [6]. The flow

reactor allows the study of the oxidation of PRF mixtures under very well-controlled, well-characterized conditions, in addition to providing valuable information of major intermediate species formed in the oxidation process. The reaction pathways responsible for the intermediate products formed will be identified and comparisons with previous studies of the oxidation of PRF mixtures in engines [20]-[27] will be made.

Previously, computed results from a lumped mechanism were compared to these experimental results for major species profiles (CO, CO_2, H_2O, O_2) [6]. The agreement was very good and provided a sound validation of the lumped model where elementary reactions in the same reaction class and isomeric species are lumped together. Lumped models are developed to reduce the computational requirements compared to detailed models. In the present work, the goal is to validate a fully detailed chemical kinetic model that is more fundamentally based on elementary reactions than lumped models. In the lumped model, both forward and reverse rates for a reaction are sometimes estimated independent of one another, so that thermodynamic principles are not always satisfied. In the detailed model the rate constant in either the forward or reverse direction is specified, usually in the exothermic direction, while the other is calculated from thermochemistry.

Chemical Kinetic Mechanism

Computer simulations were performed using the HCT modeling code [31], which solves the coupled chemical kinetic and conservation equations for energy, mass and momentum under a variety of boundary and initial conditions for reactive systems. The high-pressure reactor experiments were simulated as an adiabatic, isobaric (12.5 atm) plug flow with negligible axial diffusion of species and energy. Shock tube simulations assumed constant volume behind the reflected shock wave. The detailed chemical kinetic reaction mechanism used in these

calculations is based on previous work by the authors [32]–[40], and on the hierarchical nature of reacting systems starting with a core mechanism describing H_2/O_2 and CO oxidation. To this is added the progressively larger C_1–C_8 mechanisms. The complete model consists of approximately 1000 different chemical species and 4000 elementary reactions.

The overall flux diagram for fuel oxidation is shown schematically in Figure 1. The naming conventions used are $\dot{R}$ and $\dot{R}'$, denoting alkyl radicals or structures and Q, denoting C_nH_{2n} species or structures. At low temperatures, chain branching is mainly due to the reaction pathway leading through the ketohydroperoxide species, which forms two reactive hydroxyl radicals. As the temperature rises, chain propagation reactions of the $\dot{Q}OOH$ radical become more important, because the energy barrier associated with $\dot{Q}OOH$ scission is more easily overcome. This leads to the formation of cyclic ethers, conjugate olefins, and β–decomposition products together with only one radical species. The increasing importance of these propagation channels leads to a lower reactivity of the system, observed as the negative temperature coefficient (NTC) region. At intermediate and high temperatures, the overall reaction pathway proceeds *via* fuel decomposition and alkyl radical β-scission, proceeding rapidly to smaller olefinic and radical species. Chain branching at intermediate temperatures occurs primarily through the sequence, fuel + $H\dot{O}_2 = \dot{R} + H_2O_2$ and $H_2O_2 = \dot{O}H + \dot{O}H$, and at high temperatures through the reaction, $\dot{H} + O_2 = \dot{O} + \dot{O}H$.

In our more recent modeling work [40] we have described how we estimate rate constant expressions for important reactions associated with the oxidation mechanism. These rate expressions rely on thermodynamic parameters for reacting species to ensure correct equilibrium balance. We employ the program THERM [41], which uses group additivity rules developed by Benson [42], to evaluate thermochemical quantities for those chemical species

for which there are no available data. H/C/O groups and bond dissociation groups were updated, based on recent work by Bozzelli and coworkers [43]. A full listing of the reaction mechanism can be obtained by Internet electronic mail (curran6@llnl.gov) or on disk by writing to the authors.

Experimental

The Princeton variable pressure flow reactor provides a well-characterized environment that is designed to minimize mixing and diffusion effects. Details of the experimental apparatus have been described previously [6],[44]–[47]. Both PRF fuels and their mixtures were studied under stoichiometric oxygen to fuel ratios, at a constant molar carbon content of 1%, and with the concentration of nitrogen diluent approximately 98.3%. Experiments were performed over an initial reactor temperature range of 550–850 K, and with a constant pressure and residence time of 12.5 atm and 1.8 s, respectively. In the experiments reported here, a continuous gas sampling flow was extracted from an axial location down stream of the point where a stream of pre-vaporized fuel diluted in nitrogen, was mixed with the main carrier flow of nitrogen and the desired amount of oxygen. The sampled flow was removed and quenched utilizing a hot-water cooled, convection-quench, stainless steel sampling probe. Temperature measurements were made at the point of sample extraction using a silica coated thermocouple. The sampled gases were passed through heated (100° C) Teflon lines and through the following on-line analyzers: a Fourier transform infrared (FTIR) system to determine water, carbon monoxide and carbon dioxide; an electrochemical analyzer to determine oxygen, and non-dispersive infrared analyzers for carbon monoxide and carbon dioxide. To obtain identification of hydrocarbon species in the sampled gases, small amounts of gases were extracted from the sample stream and stored off-line in a heated, multi-loop sample valve for anal-

yses using gas chromatograph techniques. Species identifications were made using a DB-5 semi-polar column to separate the heavy components. Identification of the chemical species present was made using an FTIR detector and comparisons of detected with either spectra from known compounds or best fits against spectra from an existing library. Low molecular components were analyzed separately using a Plot Q column and flame ionization detection. Other experimental procedures were as described elsewhere [6, 46].

Discussion

Figure 2 shows comparisons of the measured and simulated reactor temperature rise as a function of initial temperature for each of the two pure PRF fuels and their mixtures. Gas temperature results from the exothermic character of the reaction process. From 560-580 K initial reaction temperature, n-heptane and the PRF mixtures begin to show some conversion, with reactivity peaking from 600–625 K due to the decomposition of ketohydroperoxide species and the formation a second reactive hydroxyl radical, resulting in chain-branching [40], [48]-[23]. At lower initial temperatures, no fuel conversion is observed because ketohydroperoxide decomposition has a high activation energy barrier of approximately 43000 cal/mol. From 600–700 K for n-heptane and 625–780 K for PRF fuel mixtures, a gradual but pronounced decrease is observed in fuel conversion. This is the characteristic NTC behavior common to paraffin fuel oxidation at low temperatures. This phenomenon is due to β-scission of $\dot{Q}OOH$ radicals which results in the formation of only one radical species in addition to cyclic ether, olefin and oxygenated β-scission products. At initial reactor temperatures above 780 K, H_2O_2 dissociates into two reactive hydroxyl radicals leading to a rapid increase in reactivity of the system and in consumption of the remaining fuel.

It appears that H_2O_2 dissociation occurs at lower initial temperatures for n-heptane than

for iso-octane and other PRF mixtures. This is because n-heptane partially reacts increasing its temperature above the initial reactor temperature. At initial temperatures above 780 K, β-scission of the larger alkyl radicals become increasingly important in comparison to addition to molecular oxygen, leading to the formation of smaller olefins, and alkyl radicals including methyl. At these conditions, the methyl radicals formed react primarily with hydroperoxy radicals, leading to the formation of methoxy and hydroxy radicals, $\dot{C}H_3 + H\dot{O}_2 = CH_3\dot{O} + \dot{O}H$ followed by $CH_3\dot{O} + M = CH_2O + \dot{H} + M$. The formaldehyde produced undergoes further reaction, primarily $CH_2O + \dot{R} = H\dot{C}O + RH$ and $H\dot{C}O + O_2 = CO + H\dot{O}_2$. At higher temperatures (>1100 K), the latter reaction is superseded by $H\dot{C}O + M = CO + \dot{H} + M$. This sequence of reactions is highly exothermic and converts relatively unreactive radicals to very reactive ones. One normally associates heat release with the $\dot{R} + O_2$ channel and notes that the β-scission channels to small olefins is nearly isoergic at low pressures. However, at high pressures, the conversion of methyl from the reaction with $H\dot{O}_2$ results in exothermicity associated with the overall β-scission process to small olefins.

Overall, there is good agreement between model predictions and experimentally measured temperature rise. The relative trends in fuel reactivity observed in the experiment are reproduced well by the detailed mechanism. The correct reactivity of n-heptane, the PRF mixtures and iso-octane is reproduced very well by the model throughout the NTC region. However, the model does not predict the low conversion of iso-octane observed at low temperatures (610–660 K). At higher temperatures (780-850 K) the model predicts the onset of the hot ignition stage which is controlled by H_2O_2 decomposition but is not quite as rapid as observed in the experiments for 87 ON PRF and iso-octane.

The detailed mechanism was also used to simulate the shock tube experiments of Fieweger

et al. [13], results of which are plotted in Figure 3. Good agreement is observed between model predicted and experimental autoignition delay times for both pure n-heptane and iso-octane fuels and their mixtures throughout the NTC region. These results were obtained using a mechanism consisting of distinct n-heptane and iso-octane sub-mechanisms. There is no interaction of either fuel other than through small radical species such as $\dot{O}H, H\dot{O}_2, \dot{O}, \dot{H}, \dot{C}H_3$ etc. This observation supports earlier work by Lee and Morley [50] and observations by Leppard [20] and Li et al. [22].

The comparisons of predicted overall reactivity with experimental observation are a good test of the kinetic mechanism but do not validate the complex chemical processes leading to partial oxidation or autoignition. To perform a more detailed test of the model we compare measured speciation data with that predicted by the model. Figure 4 shows comparisons of experimental measurements and model predictions for O_2, CO, CO_2, and H_2O species produced in 92 ON PRF mixture oxidation. The model predictions agree with the experimental results quite well, although the hot ignition stage is not quite as rapid as observed in the experiment. In addition, many larger intermediates were positively identified by matching the retention times and GC-FTIR spectral peaks to those in a library. Table 1 reports these positively identified species, together with concentrations for 92 ON PRF fuel predicted by the model. All the identified species are predicted in detectable concentrations except ethane and 4-methyl-2-pentanone. We have used the output from the detailed model to discern the various intermediates formed at 640 and 820 K and have classified them by type i.e. olefins, aldehydes, ketones, and cyclic oxygenates, in Table 2. Unreacted fuel and methane constitute the paraffinic species present. The species formed in most abundance are the small C_1 oxygenates of formaldehyde, carbon monoxide and carbon dioxide. However, it is evident

that the C_4 submechanism plays a large part in iso-octane oxidation under these conditions.

Leppard [20] performed autoignition experiments in a motored CFR engine using n-heptane, iso-octane and PRF mixtures, and speciated the exhaust gases. Leppard found that at an engine operating speed of 500 RPM, intake manifold pressure of 120 kPa and temperature of 448 K, iso-octane autoignited at a critical compression ratio (CCR) of 10.7. He also quantified the major intermediates produced at a compression ratio (CR) of 10.5, the highest operable CR without the occurence of autoignition, and reported that 36% of the fuel had reacted. The model predicts a CCR of 10.25 and that 44.5% of the fuel is oxidised. Table 3 shows experimental results together with those predicted by the detailed mechanism at 36% fuel conversion. Of the alkenes, isobutene was the largest measured component by a factor of five, with propene, di- and tri-methyl pentenes composing the remainder. The model predicts isobutene formation in greatest abundance, but propene is overpredicted by a factor of three. Of the pentenes, the predicted concentrations of 2,4-dimethyl-2-pentene, 2,4,4-trimethyl-1-pentene and 2,4,4-trimethyl-2-pentene are quite good even though the relative concentrations of the tri-methyl pentenes are reversed. In addition, 4,4-dimethyl-2-pentene is underpredicted by about an order of magnitude.

The only alkanes identified were methane (in trace amounts) and iso-octane. Of the measured oxygenates, formaldehyde, 2,2,4,4-tetramethyl-tetrahydro-furan (TMTHF) and acetone were present in the greatest amounts, followed by 2-tert-butyl-3-methyl oxetane, 2-isopropyl-3,3-dimethyl oxetane, isobuteraldehyde and methacrolein. Formaldehyde is predicted within a factor of two, while acetone is overpredicted by about an order of magnitude. TMTHF is underpredicted by less than a factor of three and the oxetanes are also underpredicted by almost an order of magnitude. Isobuteraldehyde is in good agreement, but the

model underpredicts methacrolein about a factor of three. The prediction of intermediate speciation data measured in engine experiments is extremely difficult, as the system passes through a wide range of temperature and pressure within the engine, and the exhaust flow which is analyzed here is also unsteady. We believe that overall, good agreement is observed between model prediction and experimental observation, although it is evident that some refinements are necessary in the chemistry.

Li et al. [22] also studied iso-octane autoignition in a motored, single-cylinder engine and obtained in-cylinder samples at different points prior to autoignition. They found that, compared to n-heptane, iso-octane showed considerably less reactivity with very little reaction until about 10° BTDC. Again, of the intermediates of iso-octane oxidation, isobutene is the most common, followed by TMTHF as in Leppard's experiments. The di- and trimethyl pentenes are also observed, as are the C_1 to C_4 aldehydes and C_8 oxetane species. 2,2-dimethyl propanal is also detected in trace amounts.

We have identified the major intermediate species important for PRF oxidation in engines. In the following section we use the modeling results to identify the reaction pathways that lead to their formation in the high pressure flow reactor.

Olefin formation

Computed results indicate that at both 640 and 820 K the C_8 olefins 2,4,4-trimethyl-1-pentene (jC_8H_{16}) and 2,4,4-trimethyl-2-pentene (iC_8H_{16}) are produced from the decomposition of the corresponding hydroperoxy-alkyl radical, e.g.: $dC_8H_{16}OOH - c = jC_8H_{16} + H\dot{O}_2$. In $dC_8H_{16}OOH$ – c, d refers to the carbon site with the OOH group attached and c refers to the radical site. The sites labeled a, b, c, and d refer to sites defined in Figure 5.

At 640 K the C_7 olefins are formed primarily from C_8 hydroperoxy-alkyl β-scission and

from cyclic ether oxidation with a small proportion of 4,4-dimethyl-2-pentene (oC_7H_{14}) generated from β-scission of 2,4,4-trimethyl-pent-3-yl (bC_8H_{17}) radical. Higher concentrations of C_7 olefins are formed at 820 K, mainly from the decomposition of C_8 alkyl radicals.

The olefinic species predicted in highest concentration is isobutene while isobutene oxygenates are also predicted in relatively high concentrations by the model. Analysis of reaction path edits at both 640 and 820 K indicates that isobutene is formed primarily *via* β-scission of 2,4,4-trimethyl-pent-1-yl (cC_8H_{17}) radical to form isobutene and tert-butyl radical. The tert-butyl radicals generated add to O_2 and form alkyl-peroxy radicals which isomerize to hydroperoxy-alkyl radicals and then β-scission to form isobutene and $H\dot{O}_2$ radicals. A small quantity of isobutene is also formed from β-scission of 2,4,4-trimethyl-pent-5-yl (aC_8H_{17}) to produce isobutene and iso-butyl radical, and 2,4,4-trimetyl-3-hydroperoxy-pentyl-5-yl ($bC_8H_{16}OOH - a$) radical scission to yield isobutene, isobuteraldehyde (iC_3H_7CHO) and hydroxyl radical.

$$cC_8H_{17} \longrightarrow iC_4H_8 + t\dot{C}_4H_9$$

$$t\dot{C}_4H_9 + O_2 \longrightarrow tC_4H_9\dot{O}_2$$

$$tC_4H_9\dot{O}_2 \rightleftharpoons tC_4H_8OOH - i$$

$$tC_4H_8OOH - i \longrightarrow iC_4H_8 + H\dot{O}_2$$

$$aC_8H_{17} \longrightarrow iC_4H_8 + i\dot{C}_4H_9$$

$$bC_8H_{16}OOH - a \longrightarrow iC_4H_8 + iC_3H_7CHO + \dot{O}H$$

At 640 K, because of the high energy barrier for β-scission, one expects that only addition of alkyl radicals to O_2 will occur, a behavior we observe in n-heptane oxidation [40]. The A-factor of a reaction is proportional to $e^{\frac{\Delta S}{R}}$, where ΔS is the entropy change from reactants to products. The entropy change for iso-octyl is greater than for n-heptyl β-sission reactions

and this results in much higher A-factors for iso-octyl β-decompositions. This is an important feature captured by the detailed mechanism, because β-scission of iso-octyl radicals at this temperature will result in less chain-branching and thus lower reactivity of the system relative to n-heptane oxidation under the same conditions. Other effects, such as the relative rate of alkylperoxyl radical isomerization, may also contribute to the experimentally observed reduction in reactivity for iso-octane relative to n-heptane. The reduced mechanisms of Ranzi et al. [23, 24] and Côme et al. [25, 26] consider only one generic alkyl radical β-scission reaction (in the forward, endothermic direction) for both fuels assuming that the rate constant is similar for both straight-chained and branched hydrocarbons. In the detailed mechanism, the rate constants for each *individual* β-scission reactions are estimated in the better-known reverse, exothermic direction for the addition of an alkyl radical to an olefin with the forward rate calculated from thermochemistry.

Oxygenate formation

The only C_8 oxygenated species observed in experiments and predicted by the model are cyclic ethers. High concentrations of TMTHF (iC_8eterac) were observed and are predicted in addition to lower concentrations of 2-t-butyl-3-methyloxetane (iC_8eterbd) and 2-isopropyl-3,3-dimethyloxetane (iC_8eterab). These species are predicted to be formed from the scission of the corresponding C_8 hydroperoxy-alkyl radicals, e.g. $aC_8H_{16}OOH - c = iC_8\text{eterac} + \dot{O}H$. In iC_8eterac, a and c refer to the carbon sites at which the oxygen atom is bonded (Figure 5). C_8 cyclic ethers are formed in much higher concentrations at 640 K than at 820 K as C_8 alkyl radical β-scission dominates at the higher temperature. However, the concentrations of C_3 and C_4 cyclic ethers are higher at 820 K because low temperature chemistry extends to higher temperatures for smaller species.

C_4 oxygenates are formed from the decomposition of C_8 hydroperoxy-alkyl species and stable ketohydroperoxide species as part of the low temperature mechanism. They are not formed from isobutene oxidation except for methacrolein (iC_3H_5CHO), almost half of which is formed from the methallyl radical reaction with $H\dot{O}_2$ radical to form methalloxy radical, $iC_4H_7\dot{O}$ and $\dot{O}H$ radical.

$$iC_8\text{ketab} \longrightarrow iC_3H_7CHO + t\dot{C}_3H_6CHO + \dot{O}H$$

$$iC_8\text{ketdb} \longrightarrow tC_4H_9CHO + CH_3\dot{C}HCHO + \dot{O}H$$

$$bC_8H_{16}OOH - d \longrightarrow C_3H_6 + tC_4H_9CHO + \dot{O}H$$

$$iC_8\text{ketaa} \longrightarrow dC_6H_{12}CHO - d + CH_2O + \dot{O}H$$

$$d\dot{C}_6H_{12}CHO - d \longrightarrow iC_3H_5CHO + iC_3H_7$$

$$i\dot{C}_4H_7 + H\dot{O}_2 \longrightarrow iC_4H_7\dot{O} + \dot{O}H$$

$$iC_4H_7\dot{O} \longrightarrow iC_3H_5CHO + \dot{H}$$

The ketohydroperoxide iC_8ketab, refers to the moiety in which the keto group is attached to the carbon site a and the hydroperoxy group is at site b of the paraent iso-octane molecule depicted in Figure 5.

Of the ketones, acetone is measured in the Leppard engine experiments in greatest abundance, Table 3, and is predicted in high concentrations by the model. At 640 K it is formed *via* ketohydroperoxide decomposition, addition of the $t\dot{C}_3H_6CHO$ radical to O_2 and tert-butoxy radical decomposition. At 820 K, acetone is mainly a product of isobutene oxidation.

$$iC_8\text{ketac} \longrightarrow CH_3COCH_3 + t\dot{C}_4H_8CHO + \dot{O}H$$

$$iC_8\text{ketbc} \longrightarrow CH_3COCH_3 + tC_4H_9\dot{C}O + \dot{O}H$$

$$iC_4\text{ketit} \longrightarrow CH_3COCH_3 + H\dot{C}O + \dot{O}H$$

$$t\dot{C}_3H_6CHO \longrightarrow CH_3COCH_3 + CO + \dot{O}H$$

$$tC_4H_9\dot{O} \longrightarrow CH_3COCH_3 + \dot{C}H_3$$

This result indicates the importance of the isobutene submechanism in iso-octane oxidation.

Formaldehyde is also produced in high concentrations. At 640 K it is produced mainly *via* $CH_3O_2H = CH_3\dot{O} + \dot{O}H$ followed by H-atom abstraction: $CH_3\dot{O} + O_2 = CH_2O + H\dot{O}_2$. At 820 K formaldehyde is formed mainly by the reaction of methyl radical with hydroperoxy radical to form methoxy, which decompose to formaldehyde and H atom as described earlier.

Conclusions

A detailed chemical kinetic model has been assembled to simulate autoignition and intermediate product formation for the primary reference fuels and their mixtures in spark ignition and compression ignition engines. Three sets of experimental results were used to validate the predictive capabilities of the kinetic mechanism. Experiments performed in a shock tube [13], in which autoignition delay times were recorded, were simulated using the detailed model with good agreement between experiment and model. Experiments carried out in a high pressure flow reactor [45] were used, not only to validate the prediction of correct overall reactivity, but also the identification and relative distribution of intermediate species produced during fuel oxidation. These data were supplemented by the experiments of Leppard [20] who differentiated and quantified the intermediate species produced during PRF oxidation in a motored engine. The major species observed in the experiment are also predicted in high concentrations by the kinetic mechanism. The reaction pathways leading to the major intermediate species in the flow reactor were identified. In addition, we have found that β-scission of octyl radicals occur at relatively low temperatures a phenomenon

not observed for n-heptyl radicals. This is due to the greater change in entropy for iso-octyl radical β-sission relative to n-heptyl radicals.

Acknowledgements

This study was performed under the auspices of the U.S. Department of Energy by the Lawrence Livermore National Laboratory under contract No. W–7405–ENG–48, and at Princeton under DOE Grant No. Fe-FG04-90AL65450.

References

[1] Wu, K. C., and Hochgreb, S., *Combust. Flame* 107:383–400 (1996).

[2] Eng, J. A., Leppard, W. R., Najt, P. M., and Dryer, F. L., Society of Automotive Engineers publication SAE–972888, (1997).

[3] Dec, J. E., Society of Automotive Engineers publication SAE–970873, (1997).

[4] Barnard, J. A., and Harwood, B. A., *Combust. Flame* 21:345–354 (1973).

[5] Dryer, F. L., and Brezinsky, K., *Combust. Sci. Tech.* 45:199–212 (1986).

[6] Callahan, C. V., Held, T. J., Dryer, F. L., Minetti, R., Ribaucour, M., Sochet, L, R., Faravelli, T., Gaffuri, P, and Ranzi, E., *Twenty-Sixth Symposium (International) on Combustion*, The Combustion Institute, Pittsburgh, 1996, pp. 739–746.

[7] Lignola, P. G., Di Maio, F. P., Marzocchiella, A., Mercogliano, R., and Reverchon, E., *Twenty-Second Symposium (International) on Combustion.*, The Combustion Institute, Pittsburgh, 1988, pp. 1625–1633.

[8] D'Anna, A., Mercogliano, R., Barbella, R., and Ciajolo, A., *Combust. Sci. Tech.* 83:217–232 (1992).

[9] Ciajolo, A., D'Anna, A., and Mercogliano, R., *Combust. Sci. Tech.* 90:357–371 (1993).

[10] Dagaut, P., Reuillon, M., and Cathonnet, M., *Combust. Sci. Tech.* 95:233–260 (1994).

[11] Dagaut, P., Reuillon, M., and Cathonnet, M., *Combust. Sci. Tech.* 103:315–336 (1994).

[12] Fieweger, K., Blumenthal, R. and Adomeit, G., *Twenty-Second Symposium (International) on Combustion.*, The Combustion Institute, Pittsburgh, 1984, pp. 1579–1585.

[13] Fieweger, K., Blumenthal, R. and Adomeit, G., *Combust. Flame* 109:599–619 (1997).

[14] Halstead, M. P., Kirsch, L. J., and Quinn, C. P., *Combust. Flame* 30:45–60 (1977).

[15] Park, P., and Keck, J. C., Society of Automotive Engineers publication SAE–900027, (1990).

[16] Griffiths, J. F., Halford-Maw, P. A., and Rose, D. J., *Combust. Flame* 95:291–306 (1993).

[17] Minetti, R., Carlier, M., Ribaucour, M., Therssen. E., and Sochet, L. R., *Combust. Flame*, 102:298–309 (1995).

[18] Minetti, R., Carlier, M., and Sochet, L. R., *Combust. Sci. Tech.* 113–114:179 (1996).

[19] Minetti, R., Carlier, M., Ribaucour, M., Therssen. E., and Sochet, L. R., *Twenty-Second Symposium (International) on Combustion.*, The Combustion Institute, Pittsburgh, 1996, pp. 747–753.

[20] Leppard, W. R., Society of Automotive Engineers publication SAE–922325, (1992).

[21] Filipe, D. J., Li, H. L., and Miller, D. L., Society of Automotive Engineers publication SAE–920807, (1992).

[22] Li, H. L., Prabhu, S. K., Miller, D. L., and Cernasky, N. P., Society of Automotive Engineers publication SAE–942062, (1994).

[23] Ranzi, E., Gaffuri, P., Faravelli, T., and Dagaut, P., *Combust. Flame* 103:91–106 (1995).

[24] Ranzi, E., Faravelli, T., Gaffuri, P., Sogaro, A., D'Anna, A., and Ciajola, A., *Combust. Flame* 108:24–42 (1997).

[25] Côme, G. M., Warth, V., Glaude, P. A., Fournet, R., Battin-LeClerc, F., and Scacchi, G., *Twenty-Sixth Symposium (International) on Combustion.*, The Combustion Institute, Pittsburgh, 1996, pp. 755–762.

[26] Glaude, P. A., Warth, V., Fournet, R., Battin-LeClerc, F. Côme, G. M. and Scacchi, G., *Bull. Soc. Chim. Belg.* 106:343 (1997).

[27] Roberts, C. E., Matthews, R. D., and Leppard, W. R., Society of Automotive Engineers publication SAE–962107, (1996).

[28] Chevalier, C., Warnatz, J., and Melenk, H., *Ber. Bunsenges. Phys. Chem.* 94:1362–1367 (1990).

[29] Chevalier, C., Pitz, W. J., Warnatz, J., Westbrook, C. K., and Melenk, H., *Twenty-Fourth Symposium (International) on Combustion.*, The Combustion Institute, Pittsburgh, 1992, pp. 92–101.

[30] Nehse, M., Warnatz, J., and Chevalier, C., *Twenty-Sixth Symposium (International) on Combustion.*, The Combustion Institute, Pittsburgh, 1996, pp. 773–780.

[31] Lund, C. M. and Chase, L., "HCT - A General Computer Program for Calculating Time-Dependent Phenomena Involving One-Dimensional Hydrodynamics, Transport,

and Detailed Chemical Kinetics," Lawrence Livermore National Laboratory report UCRL-52504, revised (1995).

[32] Westbrook, C. K. and Pitz, W. J., *Combust. Sci. Tech.* 37:117 (1984).

[33] Westbrook, C. K., Warnatz, J., and Pitz, W. J., *Twenty-Second Symposium (International) on Combustion.*, The Combustion Institute, Pittsburgh, 1988, pp. 893–901.

[34] Westbrook, C. K., Pitz, W. J., and Leppard, W. R., Society of Automotive Engineers publication SAE–912314, (1991).

[35] Westbrook, C. K., and Pitz, W. J., *Western States Section/ The Combustion Istitute*, 1993.

[36] Curran, H. J., Gaffuri, P., Pitz, W. J., Westbrook, C. K., and Leppard, W. R., Society of Automotive Engineers publication SAE–952406, (1995).

[37] Curran, H. J., Gaffuri, P., Pitz, W. J., Westbrook, C. K., Callahan, C., Dryer, F. L., and Held, T., *Central States/Western States/Mexican Ntl. Sections Comb. Inst.*, 1995, p. 263.

[38] Curran, H. J., Pitz, W. J., and Westbrook, C. K., Hisham, M. W. M., and Walker R. W., *Twenty-Sixth Symposium (International) on Combustion*, The Combustion Institute, Pittsburgh, 1996, pp. 641–649.

[39] Curran, H. J., Gaffuri, P., Pitz, W. J., Westbrook, C. K., and Leppard, W. R., *Twenty-Sixth Symposium (International) on Combustion*, The Combustion Institute, Pittsburgh, 1996, pp. 2669–2677.

[40] Curran, H. J., Gaffuri, P., Pitz, W. J. and Westbrook, C. K., *Combust. Flame* in press, (1998).

[41] Ritter, E. R., and Bozzelli, J. W., *Int. J. Chem. Kinet.* 23:767–778 (1991).

[42] Benson, S. W., *Thermochemical Kinetics.* John Wiley and Sons, Inc., New York, 1976.

[43] Lay, T., Bozzelli, J. W., Dean, A. M., and Ritter, E. R., *J. Phys. Chem.* 99:14514 (1995).

[44] Held, T. J., Callahan, C. V., and Dryer, F. L., The Annual Automotive Technology Development Contractor's Meeting, Dearborn, 1994, p. 257.

[45] Callahan, C. V., M. S. E. Thesis, Department of Mechanical and Aerospace Engineering, Princeton University, 1995.

[46] Held, T. J., and Dryer, F. L., *Twenty-Fifth Symposium (International) on Combustion*, The Combustion Institute, Pittsburgh, 1994, pp. 901–908.

[47] Kim, T. J., Yetter, R. A., and Dryer, F. L., *Twenty-Fifth Symposium (International) on Combustion*, The Combustion Institute, Pittsburgh, 1994, p. 759.

[48] Blin-Simiand, N., Rigny, R., Viossat, V., Circan, S., and Sahetchian, K., *Combust. Sci. Tech.*, 88:329–348 (1993).

[49] Sahetchian, K. A., Rigny, R., and Circan, S., *Combust. Flame* 85:511–514 (1991).

[50] Lee, G. R., and Morley, C., Society of Automotive Engineers publication SAE–941958, (1994).

Figure Captions

Figure 1: Schematic representation of the primary oxidation reactions.

Figure 2: PRF oxidation at 12.5 atm, $\phi = 1.0$, $\tau = 1.8$ s, 98.3% N_2. Experimental (symbols) [6] vs. model predicted temperature rise in reactor as a function of inlet reactor temperature. Dotted lines correspond to open symbols.

Figure 3: PRF oxidation at 40 atm, stoichiometric fuel in air. Experimental (symbols) [13] vs. model predicted ignition delay times. Dotted lines correspond to open symbols.

Figure 4: 92 ON oxidation at 12.5 atm, $\phi = 1.0$, $\tau = 1.8$ s, 98.3% N_2. Experimental (symbols) [6] vs. model predicted species concentrations as a function of inlet reactor temperature. Dotted lines correspond to open symbols.

Figure 5: Iso-octane with its four distinct sites for H-atom abstraction. 12.5 atm, $\phi = 1.0$, $\tau = 1.8$ s.

92 ON PRF Intermediates	Model Predicted Species Mole Fraction
formaldehyde	2.87e-4
ethane	9.04e-8
propene	7.50e-5
isobutene	2.34e-4
acetone	1.56e-4
isobuteraldehyde	2.28e-5
methacrolein	3.90e-6
2,2-dimethyl propanal	2.95e-5
4,4-dimethyl-2-pentene	1.80e-6
2,4-dimethyl-2-pentene	3.25e-6
2,4,4-trimethyl-1-pentene	4.89e-5
2,4,4-trimethyl-2-pentene	4.44e-5
4-methyl-2-pentanone	2.63e-8
2,2,4,4-tetramethyl-THF	1.02e-4

Table 1: Comparison of major intermediates positively identified by GC-FTIR and predicted by the model. 92 ON oxidation at 12.5 atm, $\phi = 1.0$, $\tau = 1.8$ s, T = 640 K, 1.0% carbon.

Predicted species formed	Reactor Temperature 640 K	820 K
Olefin		
propene	7.50e-5	3.59e-4
isobutene	2.34e-4	5.48e-4
2-methyl-1-pentene	3.58e-6	8.30e-6
2,4-dimethyl-1-pentene	8.94e-7	8.80e-6
2,4-dimethyl-2-pentene	3.25e-6	6.87e-5
4,4-dimethyl-1-pentene	2.36e-6	4.43e-5
4,4-dimethyl-2-pentene	1.80e-6	1.19e-5
2,4,4-trimethyl-1-pentene	4.89e-5	2.61e-6
2,4,4-trimethyl-2-pentene	4.44e-5	1.34e-5
Aldehyde		
formaldehyde	2.87e-4	4.82e-4
acetaldehyde	3.58e-5	1.77e-5
isobuteraldehyde	2.28e-5	1.62e-5
methacrolein	3.90e-6	8.19e-6
pentanaldehyde	2.67e-6	—
2,2-dimethyl propanal	2.95e-5	—
Ketone		
acetone	1.56e-4	8.12e-5
2-pentanone	6.48e-6	—
4-methyl-2-pentanone	2.63e-8	—
2,4-dimethyl-3-pentanone	6.89e-6	—
2,2-dimethyl-3-pentanone	3.74e-6	—
4,4-dimethyl-2-pentanone	1.51e-6	—
Cyclic ether		
2-methyl oxirane	1.86e-6	2.86e-5
isobutene oxide	3.42e-6	6.73e-5
2,4,4-trimethyl-THF	1.85e-6	—
2-propyl-THF	1.87e-6	—
2-methyl,5-ethyl-THF	4.23e-6	1.37e-6
2,2,4,4-tetramethyl-THF	1.02e-4	1.31e-6
2-t-butyl-3-methyl-oxetane	3.81e-6	—
2-isopropyl-3,3-dimethyl-oxetane	3.77e-6	—

Table 2: Model predicted mole fractions of major intermediates produced in a flow reactor. 92 ON oxidation at 12.5 atm, $\phi = 1.0$, $\tau = 1.8$ s, 1.0% carbon.

Iso-octane Intermediates	Species Mole Fraction	
	Experiment	Model Prediction
carbon monoxide	2.310e-3	3.29e-3
isobutene	1.694e-3	3.72e-3
formaldehyde	1.170e-3	2.89e-3
2,2,4,4-tetramethyl-THF	1.011e-3	3.82e-4
acetone	8.180e-4	8.65e-3
2-t-butyl-3-methyloxetane	5.510e-4	1.85e-5
2-isopropyl-3,3-dimethyloxetane	4.740e-4	5.16e-5
propene	3.230e-4	1.09e-3
4,4-dimethyl-2-pentene	2.520e-4	3.45e-5
2,4,4-trimethyl-1-pentene	2.320e-4	5.14e-4
isobuteraldehyde	2.070e-4	3.11e-4
methacrolein	1.860e-4	6.57e-5
2,4-dimethyl-2-pentene	1.680e-4	1.49e-4
2,4,4-trimethyl-2-pentene	1.520e-4	5.49e-4
2,3-epoxy-2,4,4-trimethylpentane	1.430e-4	1.11e-5
isobutene oxide	1.390e-4	1.02e-4
2,2-dimethyl propanal	1.300e-4	2.34e-4

Table 3: Comparison of major intermediates formed in a CFR engine at 36% fuel conversion. Iso-octane, $\phi = 1.0$, 500 RPM.

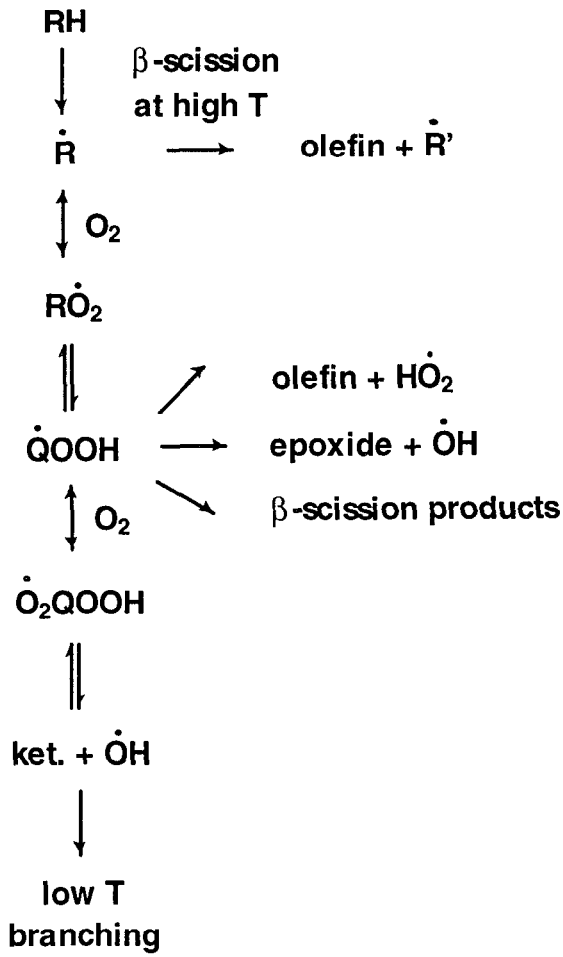

Figure 1: Schematic representation of the primary oxidation reactions

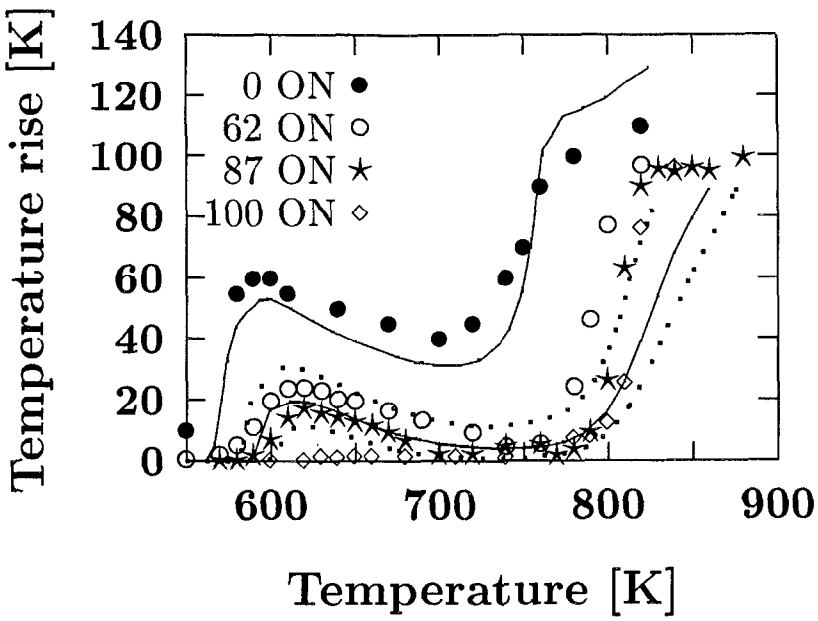

Figure 2: PRF oxidation at 12.5 atm, $\phi = 1.0$, $\tau = 1.8$ s, 98.3% N_2. Experimental (symbols) [6] vs. model predicted temperature rise in reactor as a function of inlet reactor temperature. Dotted lines correspond to open symbols.

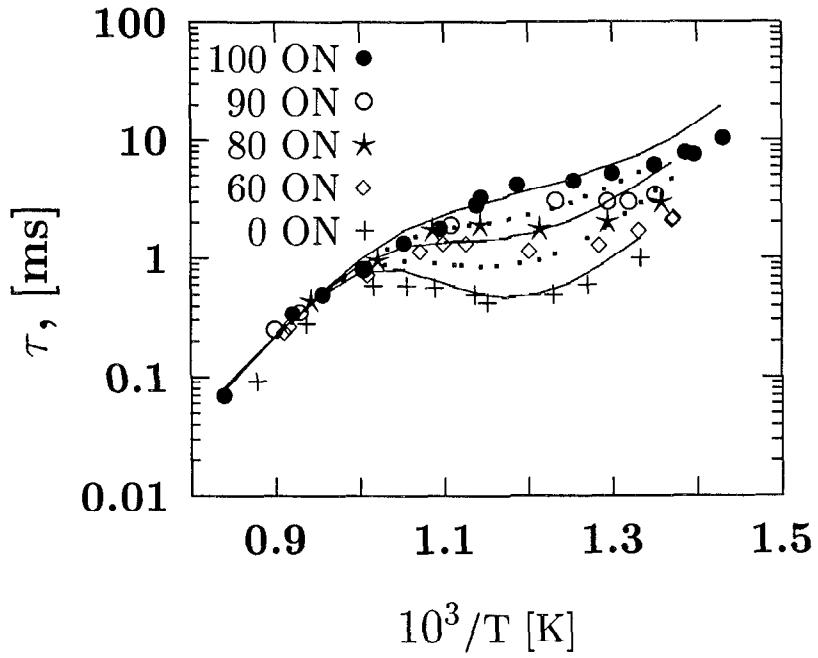

Figure 3: PRF oxidation at 40 atm, stoichiometric fuel in air. Experimental (symbols) [13] vs. model predicted ignition delay times. Dotted lines correspond to open symbols.

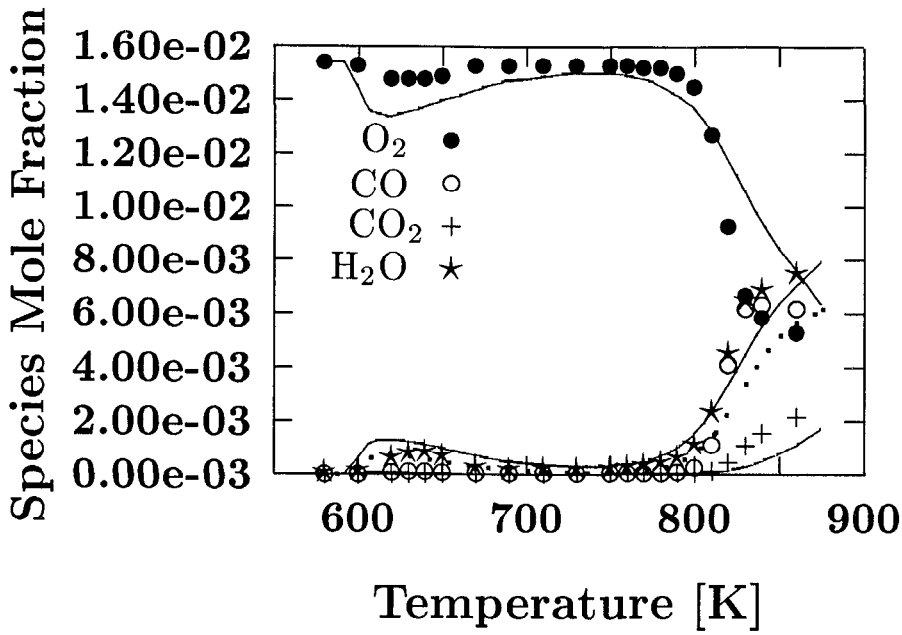

Figure 4: 92 ON oxidation at 12.5 atm, $\phi = 1.0$, $\tau = 1.8$ s, 98.3% N_2. Experimental (symbols) [6] vs. model predicted species concentrations as a function of inlet reactor temperature. Dotted lines correspond to open symbols.

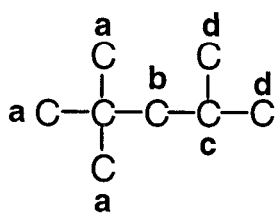

Figure 5: Iso-octane with its four distinct sites for H-atom abstraction.

Technical Information Department • **Lawrence Livermore National Laboratory**
University of California • Livermore, California 94551